Molecular rotors provide insights into microscopic structural changes during protein aggregation

Alexander J. Thompson[1†], Therese W. Herling[2†], Markéta Kubánková[1], Aurimas Vyšniauskas[1], Tuomas P. J. Knowles[2*], Marina K. Kuimova[1*]

[1]Chemistry Department, Imperial College London, Exhibition Road, London SW7 2AZ, UK

[2]Department of Chemistry, University of Cambridge, Lensfield Road, Cambridge CB2 1EW, UK

ABSTRACT: Changes in microscopic viscosity represent an important characteristic of structural transitions in soft matter systems. Here we demonstrate the use of molecular rotors to explore the changes in microrheology accompanying the transition of proteins from their soluble states into a gel phase composed of amyloid fibrils. The formation of beta-sheet rich protein aggregates – including amyloid fibrils – is a hallmark of a number of neurodegenerative disorders and, as such, the mechanistic details of this process are actively sought after. In our experiments, molecular rotors report an increase in rigidity of approximately three orders of magnitude during the aggregation reaction. Moreover, phasor analysis of the fluorescence decay signal from the molecular rotors suggests the presence of multiple distinct mechanistic stages during the aggregation process. Our results show that molecular rotors can reveal key microrheological features of protein systems not observable through classical fluorescent probes operating in light switch mode.

INTRODUCTION

The propensity of proteins to misfold and self-assemble into fibrillar nanostructures is associated with a range of increasingly prevalent neurodegenerative disorders such as Alzheimer's and Parkinson's disease[1-3]. Due to this connection with pathology and the fundamental interest of such structures for normal and aberrant biology[4], a range of experimental techniques has been developed to probe the mechanistic details of amyloid formation. The change in the fluorescence spectrum of small synthetic fluorophores upon interaction with amyloid fibrils has been a key probe that has enabled the effect of solution conditions on aggregation to be investigated *in vitro* and the identification of amyloid plaques[5] in diseased tissues. In particular, the increase in the fluorescence quantum yield of Thioflavin T (ThT) upon binding to amyloid structures underlies its action as a light switch and is the basis of its use as a common reporter of amyloid formation[6, 7]. However, the specific site and the detailed mechanism of the interaction between ThT and amyloid fibrils have remained challenging to identify. Consequently, it is in general not straightforward to obtain a clear quantitative relationship between the absolute ThT fluorescence intensity and the quantity of amyloid material formed[8]. Furthermore, the fluorescence intensity of these light switch fluorophores usually only reports on the formation of a single species, often the final fibrillar state, and does not reveal the presence of oligomers or other types of aggregates.

It has been suggested that the fluorescence lifetime of ThT may provide some additional information about the aggregation of insulin (compared to intensity measurements)[9]. Mohanty *et al*[9] reported that three components were required to accurately fit ThT fluorescence decays recorded in aggregating insulin. Noting that the ThT decays in homogeneous solution are bi-exponential[10], this data indicates a complex composition of the aggregation mixture. None the less, the limitations to light switch techniques are clear and significant efforts have recently been focussed on exploring alternative reporter molecules with more specific changes in their spectra, including conformation sensitive luminescent polyelectrolytes[11] and dyes that fluoresce in the presence of oligomers or fibrils but not in the presence of monomers[12]. Additionally, attempts have also been made to monitor amyloid formation using intrinsic protein fluorescence (e.g. [13, 14]) or using more sophisticated optical approaches, such as fluorescence

correlation spectroscopy (FCS)[15], raster image correlation spectroscopy (RICS)[16, 17], fluorescence anisotropy[18-20], fluorescence recovery after photobleaching (FRAP)[20] and single molecule detection based on Förster resonance energy transfer (FRET)[21]. These methods provide alternative techniques with which to follow protein aggregation – both in solution and in live cells – and some offer opportunities to correlate the aggregation state to the diffusion coefficients of exogenous fluorophores. However, fluorescence intensity based (light switch) measurements remain the gold standard for monitoring protein aggregation. Hence, further development of novel techniques to monitor protein aggregation is still required.

Here we present a new optical approach for probing protein aggregation processes, which relies upon measurements of the fluorescence lifetime of a molecular rotor. Molecular rotors are fluorophores that are sensitive to the viscosity of their local microscopic environment, with an increase in the local viscosity resulting in an increase in the fluorescence quantum yield – and, hence, the fluorescence lifetime – of the rotor. Unlike conventional light switch molecules, however, this increase does not rely on specific interactions with the aggregating protein but rather reports on the degree of crowding and microviscosity in the molecular environment of the rotor. We hypothesised that this method has the potential to identify intermediate structures and transiently populated states during the course of an aggregation reaction due to the different microenvironments these provide for the rotor.

The viscosity sensitivity of molecular rotors is based on the dependence of their non-radiative decay rates on the viscosity of the local environment[22-24]. In a low viscosity environment the fluorescence from the rotor is typically low. By contrast, in viscous media, the intramolecular rotation that promotes non-radiative decay is restricted, and fluorescence becomes the preferred deactivation pathway of the photo-excited state. This effect leads to an increase in the fluorescence lifetime (τ_f) as a function of increasing viscosity, which provides the basis for a quantitative determination of microviscosity as, crucially, the fluorescence lifetime is not reliant on fluorophore concentration in the same way that the fluorescence intensity is.

During protein aggregation, the effective viscosity reported by the molecular rotors might be influenced by two independent factors. First, structural changes occurring as the proteins aggregate will cause changes in microviscosity (or solution free volume), as larger and more ordered structures are likely to present a more restricted environment for the molecular rotors. Second, if the binding affinities of the molecular rotor for the various constituents of the aggregation mixture (i.e. monomers, oligomers, fibrils, etc.) are different, then the viscosity reported by the rotor in the presence of each constituent will also be different. In this case, a higher binding affinity will lead to a higher reported viscosity.

As such, by using a molecular rotor that does not show strong, specific interactions with amyloid fibrils (relative to other constituents of the aggregation mixture), it becomes possible to probe the microstructure of all components involved in the aggregation process and to monitor the dynamics of their interconversion. Importantly, this is not possible with standard light switch dyes, which typically report only on the presence of the end product of the aggregation reaction (mature amyloid fibrils).

We note that our method will not produce results of a quantitative nature if there is strong, specific binding between the rotor and the protein molecules. For example, there is evidence that ThT is itself a molecular rotor[10, 25, 26], however, as it binds strongly to many amyloid fibrils, it reports predominantly on the presence of fibrillar structures. This effect and its implications for the sensing capabilities of both ThT and the molecular rotor used in this study are discussed in detail below.

In this work we have used fluorescence lifetime imaging and phasor analysis[27] of the molecular rotor $DiSC_2(3)$ (3,3′-Diethylthiacarbocyanine iodide) to study the aggregation of the proteins lysozyme and insulin *in vitro*. Self-assembly of lysozyme is associated with systemic amyloidosis[28, 29] and represents a well characterised system for probing protein aggregation *in vitro*. We have also applied this technique to investigate insulin aggregation and demonstrate its potential for wide-ranging applications in the study of amyloid formation. In both lysozyme and insulin, we have compared our results to data obtained using identical analysis of ThT, a widely used light switch sensor for the presence of fibrillar amyloids. Our results indicate that the use of a functioning molecular rotor has the potential to provide important new insights into the mechanism of protein aggregation that are not available using current techniques.

RESULTS AND DISCUSSION

Viscosity calibration of $DiSC_2(3)$

$DiSC_2(3)$ has previously been reported as a molecular rotor that reports microviscosity through its fluorescence lifetime[30]. To permit quantitative measurements of viscosity during aggregation, we first measured fluorescence decays from $DiSC_2(3)$ in methanol/glycerol solutions of known viscosity (Fig. 1a). The decays measured under these conditions were well described by a mono-exponential model and the lifetime increased with increasing viscosity, conforming to the equation shown in Fig. 1b. In this manner, we generated a calibration dataset, which allowed quantitative conversion between the measured lifetimes and the local viscosity. The phasor representation[27] (see below) of the measured decays is shown in Fig. 3b.

Lysozyme aggregation studied using $DiSC_2(3)$

We then acquired, as a function of time, fluorescence lifetime images of $DiSC_2(3)$ in lysozyme solutions undergoing aggregation, using a multiphoton microscope. We initiated the aggregation reaction by mixing a small fraction of pre-formed seed aggregates (2.4% w/w of the total monomer concentration) with a solution of lysozyme protein. To promote amyloid fibril growth the aggregation time courses were monitored under conditions of low pH and elevated temperature[31, 32]. Our observations show that a typical time course of lysozyme aggregation proceeds through different stages. Initially no structural features are visible in the multiphoton fluorescence images (Supplementary Fig. 1a) and the fluorescence decays are dominated by a short lived component (Supplementary Fig. 2a). Subsequently, micron scale structures are visualised by monitoring the rotor fluorescence (Supplementary Fig. 1b-d) and the fluorescence lifetimes are observed to increase as the protein aggregates grow and form a stable network over time (Fig. 2a&b, Fig. 3a and Supplementary Fig. 2a). This increase in lifetime indicates a global increase in viscosity or a higher order of rigidity brought about by changes in microscopic structure.

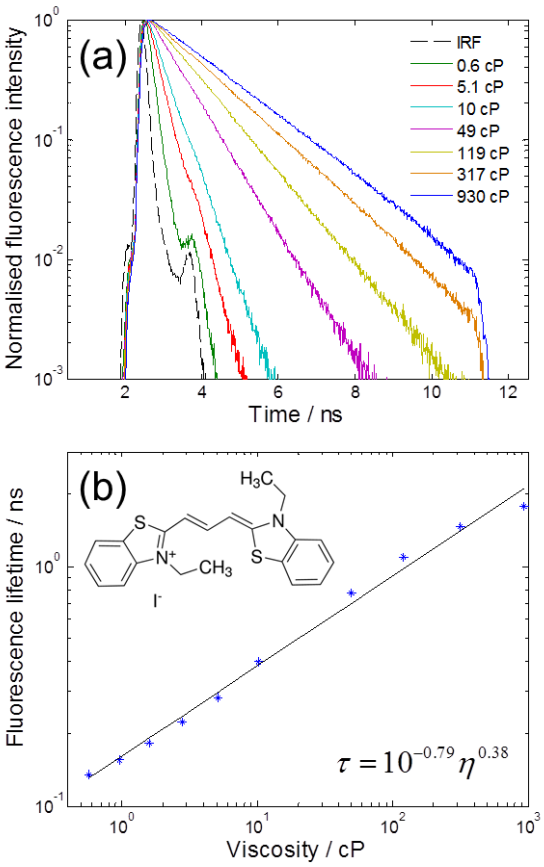

Figure 1. Viscosity calibration of the fluorescence lifetime of $DiSC_2(3)$. **a**, Fluorescence decays from $DiSC_2(3)$ in methanol/glycerol mixtures of varying concentrations. Viscosities are shown in the key. **b**, Log-log graph of fluorescence lifetime – obtained from a mono-exponential fit of the data shown in (**a**) – against viscosity showing a linear relationship across a wide range of viscosities. Inset are the chemical structure of $DiSC_2(3)$ and the Förster-Hoffmann viscosity-lifetime calibration equation for $DiSC_2(3)$, corresponding to the black line.

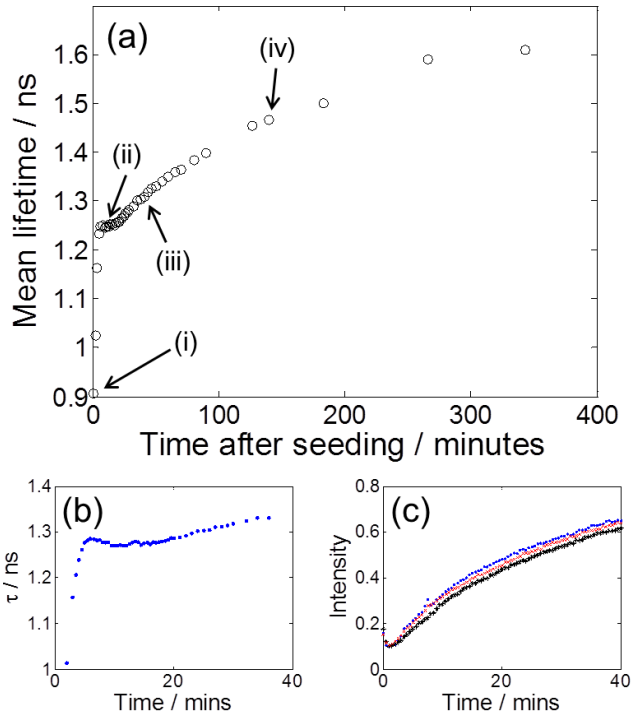

Figure 2. Evolution of the mean fluorescence lifetime of $DiSC_2(3)$ in aggregating lysozyme (4 mg/ml monomeric lysozyme, 50 mM HCl, 100 mM NaCl, 0.2% v/v DMSO, 2.4% w/w sonicated pre-formed fibrils). **a**, Mean fluorescence lifetime of $DiSC_2(3)$ as a function of time through the aggregation reaction. Measurements were made at 1.5 minute intervals for 29 minutes then less frequently for the remainder of the experiment. The acquisition time was 60 s in all cases. Roman numerals indicate the time points corresponding to the fluorescence lifetime images shown in Fig. 3a. **b**, Mean fluorescence lifetime observed in a repeat experiment with higher temporal resolution (10 s acq. time, 30 s between measurements). **c**, Normalised ThT fluorescence intensity curves measured in three repeat lysozyme aggregations (conditions as above). Note that the mean fluorescence lifetime of $DiSC_2(3)$ (**a**, **b**) reveals more structure than the ThT intensity data (**c**).

A quantitative analysis of the decays (involving bi-exponential fitting) reveals the presence of multiple lifetimes at all aggregation stages (Supplementary Figs. 2-4). Additionally, the evolution of the mean fluorescence lifetime of DiSC2(3) (Fig. 2a&b) exhibits more structural detail than standard ThT intensity curves recorded on an identical sample (Fig. 2c). The mean fluorescence lifetime increases non-monotonically with time (Fig. 2a&b) and there appear to be several distinct stages to the aggregation reaction, each exhibiting a different rate of change in mean lifetime. These stages are particularly clear in Fig. 2b (which has a higher temporal resolution than Fig. 2a) where a partial decrease in the mean lifetime

is observed after the initial sharp rise (0-5 min). Additionally, throughout the aggregation reaction the fluorescence intensity of DiSC2(3) increased in a manner broadly similar to that of the mean lifetime (Fig. 2a&b), however, the structural detail described above was less apparent (Supplementary Fig. 4c&d).

To unravel this mechanistic complexity we used phasor analysis[27], which considers the real and imaginary parts of the time domain Fourier transform of the fluorescence decay obtained via time correlated single photon counting at a fixed frequency, ω, determined by the laser repetition rate (80 MHz). For systems characterised by a single lifetime, τ, the phasor points $g(\omega) = 1/[1 + (\omega\tau)^2]$ and $s(\omega) = \omega\tau/[1 + (\omega\tau)^2]$ fall on the so-called 'universal circle' – a semicircle of radius ½, centred on g = ½, s = 0 (for example, see the $DiSC_2(3)$ calibration dataset in Fig. 3b). In this representation, the shortest lifetimes ($\tau \rightarrow 0$) approach the point g = 1, s = 0, with longer lifetimes resulting in phasor points moving anticlockwise around the universal circle. Importantly, phasor analysis is a model-free strategy that does not require any fitting or any prior knowledge of the number of fluorescent components or their respective lifetimes. Thus, this approach allows us to determine the minimum number of constituents (with distinct fluorescence lifetimes) that are present in an aggregation reaction, without relying on assumptions that are inherent in exponential fitting regimes (e.g. if we assume a 3-component decay then the fitting procedure will return a 3-component fit).

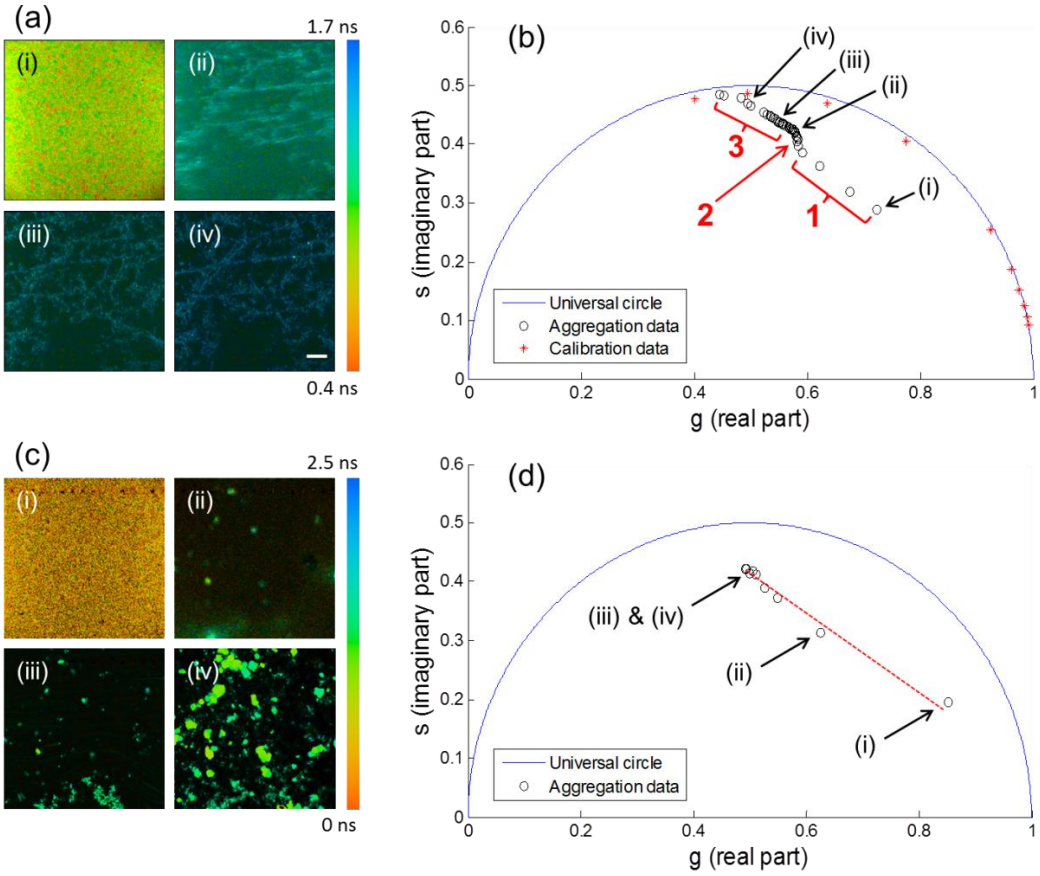

Figure 3. Multiphoton fluorescence lifetime imaging microscopy and phasor analysis of $DiSC_2(3)$ (a, b) and ThT (c, d) in aggregating lysozyme (4 mg/ml monomeric lysozyme, 50 mM HCl, 100 mM NaCl, 0.2% v/v DMSO, 2.4% w/w sonicated pre-formed fibrils). **a**, Representative $DiSC_2(3)$ fluorescence lifetime maps of aggregating lysozyme recorded (i) 50 seconds, (ii) 15.5 minutes, (iii) 41 minutes and (iv) 140 minutes after the sample was seeded with 2.4% w/w sonicated pre-formed fibrils. Images were recorded at 1.5 minute intervals for 29 minutes then less frequently for the remainder of the experiment and the acquisition time was 60 s in all cases. Scale bar in (iv) is 100 µm in length and is representative of all images shown in both (**a**) and (**c**). Fluorescence lifetime is represented by the false colour scale displayed to the right of the images. **b**, Phasor plot showing the evolution of the centroids of the phasor clouds (Supplementary Fig. 3a) recorded during the course of aggregation (open black circles). The methanol-glycerol calibration data for $DiSC_2(3)$ is also shown (red asterisks). Roman numerals indicate the centroids corresponding to the images shown in (**a**). The bold numbers shown in red indicate the three stages of the aggregation, referred to in the main text as 1, 2, and 3. **c**, Representative ThT fluorescence lifetime maps from a repeat lysozyme aggregation reaction recorded (i) before seeding and then (ii) 140 seconds, (iii) 10 minutes and (iv) 100 minutes after the sample was seeded. Conditions for the reaction monitored using ThT were identical to those for the reaction shown in (**a**) and (**b**). **d**, Phasor plot showing the evolution of the centroids of the ThT phasor clouds recorded during aggregation. Roman numerals indicate the centroids corresponding to the images shown in (**c**). Using ThT, a near-linear progression is observed on the phasor plot (red dotted line) in contrast to the multiple stages observed with $DiSC_2(3)$.

To our knowledge, phasor analysis has only been previously applied to the study of protein aggregation once[33], where the authors measured fluorescence decays from tryptophan residues in lysozyme during its aggregation. This approach revealed differences in the phasors of aggregates formed under different conditions. However, it did not elucidate any novel detail about the aggregation process, nor did it provide measurements of the mechanical properties of the aggregating solutions. As explained below, combining phasor analysis with the use of a functioning molecular rotor provides both of the above.

Using this strategy, we recorded fluorescence lifetime images (Fig. 3a) and computed the phasor points for each pixel of the spatially resolved lifetime maps (Supplementary Fig. 3a). Interestingly, the phasor clouds are not localised on the universal circle, indicating the presence of multiple components. Moreover, the clouds progress from the lower right to the upper left of the phasor plot as the aggregation proceeds, indicating a global increase in rigidity. A detailed examination of the time evolution of the phasors corresponding to samples with an increasing degree of aggregation, shown in Fig. 3b, reveals that the reaction progresses through three distinct stages, depicted as 1-3 on the graph. By contrast, following the aggregation reaction through the conventional light switch fluorescence of ThT results in a simple monotonically increasing curve without the structural detail afforded by phasor analysis (or exponential fitting) of the molecular rotor data (Fig. 2c and Supplementary Fig. 5).

We have confirmed that $DiSC_2(3)$ itself did not affect the rate of aggregation as reported by ThT (Supplementary Fig. 6). This data confirms that the structural features observed using phasor analysis of $DiSC_2(3)$ are an intrinsic property of lysozyme aggregation and are not introduced by the molecular rotor itself.

In the phasor representation, points lying on a straight line inside the universal circle correspond to mixtures of the two components at the extremities of the straight line (the points at which it intersects the universal circle). The $DiSC_2(3)$ data in Fig. 3b show that stage 1 of the lysozyme aggregation reaction represents a linear progression inside the universal circle and, as such, corresponds to conversion between two species. In order to gain insight into the nature of the two interconverting species, we measured the phasor points corresponding to the aggregation solution with no protein, soluble (monomeric) lysozyme and a suspension of seed fibrils, prepared through sonication of fully aggregated fibrils. The results in Fig. 4a show that the phasor point of the solution containing no protein lies on the universal circle as expected for a single component mixture, with a viscosity close to that of pure water. Both the monomeric lysozyme solution and seed sample lie on the same straight line observed in stage 1 of the aggregation reaction. The lysozyme solution lies closer to the low-viscosity end point of the straight line than either the seed sample or any of the aggregating mixtures. Moreover, the straight line observed in stage 1 intersects the universal circle at the phasor point corresponding to the reaction mixture containing no protein (0.6 cP, labelled '*M*' on Fig. 4a) and at a second intersection point corresponding to a high viscosity (400 cP) solution (labelled '*X*'). Thus, stage 1 corresponds to the direct transition from a low viscosity sample consisting of soluble protein to a high rigidity fibrillar system. This finding is consistent with the continuous increase in ThT fluorescence observed over the same timescale (Fig. 2c and Supplementary Fig. 5), indicating the growth of amyloid fibrils.

We further confirmed our assignment of the nature of stage 1 by performing a titration of a buffered $DiSC_2(3)$ solution with aliquots of fully formed lysozyme fibrils (Fig. 4b). The near straight line observed in this case overlaps well with stage 1 of the aggregation reaction, reaffirming that this first stage involves a direct transition from monomers to fibrils. Additionally, the fact that a near linear progression is obtained in the titration experiment indicates that stage 2 of the aggregation reaction corresponds to the formation of a new species – other than monomers or fibrils – the appearance of which causes a marked non-linearity in the phasor trajectory.

The beginning of stage 3 in the phasor diagram coincides with the change in morphology observed in the spatially resolved fluorescence lifetime images. Indeed, at this point, the solution undergoes a transition from a homogeneous state, as resolved with diffraction limited multiphoton fluorescence microscopy, to a system with visible structure on the micron scale. As such, stage 2 (the upward movement connecting stages 1 and 3) in the phasor diagram can be identified with the formation of a third microenvironment for the rotors (due to the deviation from the linear trajectory observed in stage 1), associated with the appearance of higher order structures. We note that this sensitivity to a third microenvironment (i.e. sensitivity to components other than monomers and mature fibrils) suggests that our novel approach has the potential to detect low molecular weight intermediate species (e.g. oligomers) that form during the course of aggregation. However, our sample was seeded, biasing the early reactions toward seed fibril elongation rather than the formation of short chain polymers (i.e. oligomers) and we believe that oligomers were not observed in this case. Finally, during stage 3, the system progresses to a gel with a high viscosity – initially in a linear manner in phasor space – eventually lying close to the universal circle, indicating a system with a dominant environment characterised by a viscosity three orders of magnitude higher than that of the initial reaction mixture.

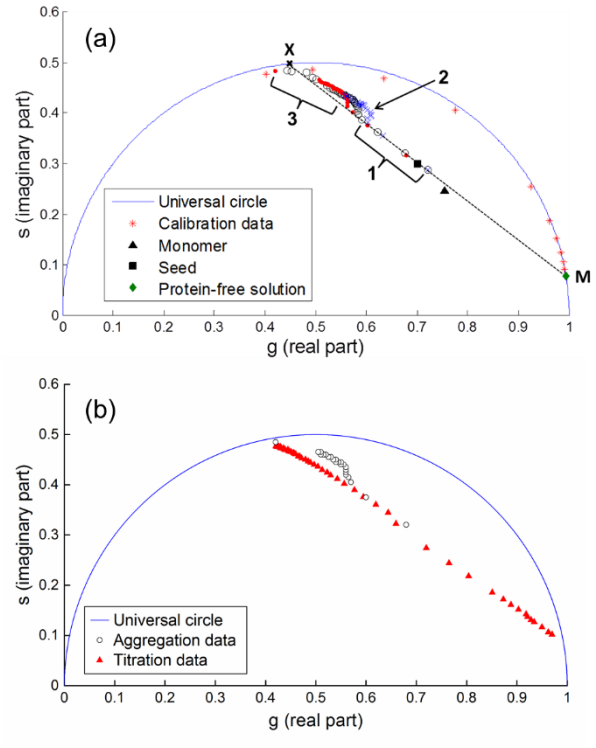

Figure 4. a, Effect of ionic strength on the aggregation of lysozyme monitored by $DiSC_2(3)$. Three experiments are shown, performed at 50 mM (x), 100 mM (○) and 200 mM (●) NaCl. All aggregations were carried out at 50 mM HCl. The calibration data for $DiSC_2(3)$ and the sample data for monomer, seed and protein-free (50 mM HCl, 100 mM NaCl only) solutions are also shown (see key). Annotations on the graph show the locations of the phasors for the components *'M'* and *'X'*, as well as the three aggregation stages (1, 2 and 3), as discussed in the text. The dotted black line indicates that stage 1 predominantly involves the reaction $M \rightarrow X$. Additionally, the phasor of component *'M'* coincides with the phasor of the protein-free solution. The position of stage 2 is altered by the addition of NaCl. **b, Comparison of a lysozyme aggregation time course and a titration of $DiSC_2(3)$ with fully formed fibrils.** The aggregation shown (○) is identical to that in (**a**), recorded at 100 mM NaCl. A titration experiment (▲) was performed by adding aliquots of fully formed lysozyme fibrils from an overnight 100 mM NaCl aggregation to an aqueous buffered solution of $DiSC_2(3)$.

Direct comparison of $DiSC_2(3)$ and ThT

We observed that lysozyme aggregation monitored using the fluorescence intensity of ThT (Fig. 2c and Supplementary Fig. 5) does not display the same level of complexity as when monitored with $DiSC_2(3)$. To provide a more complete comparison of the molecular rotor $DiSC_2(3)$ with ThT, we also recorded multiphoton fluorescence lifetime images of ThT in the presence of aggregating lysozyme. The fluorescence lifetime maps and phasor trajectories obtained in two representative lysozyme aggregation reactions monitored with ThT are shown in Fig. 3c&d and Supplementary Fig. 7.

In these reactions an increase in lifetime is observed as fibrils form. However, the phasor trajectories observed for ThT exhibit only one distinct stage. In Fig. 3d, the centroids of the measured phasor clouds progress linearly from a starting point at the bottom right of the phasor plot to an end point in the upper central region. The formation of fibrillar structures is observed as this linear progression takes place (Fig. 3c). These results suggest that, similarly to $DiSC_2(3)$, ThT acts as a molecular rotor and senses an increase in the viscosity of its micro-environment during the course of the lysozyme aggregation reaction. However, phasor points lying on a straight line inside the universal circle correspond to mixtures of two components only. This near linear ThT progression is also reminiscent of the results of the titration of $DiSC_2(3)$ with fully formed fibrils, shown in Fig 4b. As such, this data indicates that ThT is only sensitive to two species involved in the reaction: monomers and mature fibrils. There are small deviations from the straight line in Fig. 3d (red dotted line), which could be due to small contributions from intermediate aggregation constituents (i.e. components other than monomers and fibrils). However, ThT has very low levels of sensitivity (if any) to such intermediates (which explain why the deviations from the linear trajectory are very small). This observation is consistent with the simple, monotonic curves observed in the aggregation reactions monitored via ThT fluorescence intensity (Fig. 2c). In contrast, the aggregation phasor trajectory observed using $DiSC_2(3)$ exhibits a much more complex structure than that recorded using ThT. Hence, it is clear that ThT does not reveal the level of mechanistic detail provided by $DiSC_2(3)$.

We note that in some cases, once the lysozyme sample is seeded, the phasor clouds of ThT progress so quickly to the end point that it is not possible to observe any intermediate points in the trajectory (Supplementary Fig. 7). Importantly, the phasor centroids reach the end point even before fibrils are discernible in the fluorescence lifetime images (Supplementary Fig. 7a(ii)). This suggests that as soon as mature fibrils are present in the aggregation mixture, ThT reports only on their presence. This is probably due to the high affinity that ThT has for fibrils and (as a result) the large increase that is observed in its fluorescence intensity when it is in the presence of fibrils rather than monomers (or, indeed, any intermediate component). $DiSC_2(3)$, on the other hand, exhibits a non-linear phasor trajectory implying sensitivity to more than two aggregation components. In turn, this implies that its affinity for mature lysozyme fibrils is lower than ThT as the fibrillar components do not dominate the fluorescence signal until a relatively late stage in the aggregation.

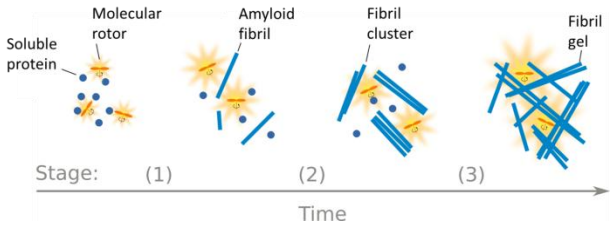

Figure 5. Illustration of the behaviour of the molecular rotors in the three observed stages of protein aggregation. The fluorescence intensity and lifetime of the rotors increase as the protein molecules aggregate and the molecular environment becomes more crowded.

Effect of ionic strength on the aggregation of lysozyme

To utilise the sensitivity of $DiSC_2(3)$ to intermediate species formed in the course of lysozyme aggregation and to explore the effect of varying conditions on the aggregation pathway, we monitored reactions at three different NaCl concentrations (Fig. 4a). Increased ionic strength was observed to globally accelerate the aggregation process (Supplementary Figs. 5 and 8), in agreement with increased ionic screening facilitating the assembly of charged proteins. Furthermore, phasor analysis reveals that the three characteristic stages discussed above are conserved even when the ionic strength of the solution is varied and the viscosity of the fully aggregated system is very similar in all cases (Fig. 4a and Supplementary Fig. 8). However, the increase in NaCl concentration results in stage 2 of the aggregation reaction being shifted towards longer lifetimes and higher viscosities. This suggests that high ionic strength favours pathway 1, as this is active for a larger fraction of the total duration of the reaction at higher NaCl concentrations.

Taken together, these data suggest that aggregation is driven by three key events. Initially, the growth of filaments in solution dominates, leading to a progressive incorporation of protein molecules into elongating amyloid fibrils (Figs. 3b and 4a, stage 1). In the second stage (Figs. 3b and 4a, stage 2), these filaments come together to form superstructures with dimensions on the micron scale, producing visible inhomogeneity in the observed fluorescence images (Fig. 3a(ii) and Supplementary Fig. 1b). Finally, the densely packed fibril networks continue to grow, depleting the monomeric protein from the soluble phase and resulting in a gel phase characterised by a single dominant microviscosity (Fig. 5). Interestingly, the three observed stages of aggregation do not correspond to a linear $A \rightarrow B \rightarrow C$ process (i.e. monomer → oligomer → polymer or monomer → fibril → gel) as a reaction of this kind would produce a completely different phasor plot trajectory, as shown in Supplementary Fig. 9. Uniquely, our molecular rotor-based approach reports on these distinct processes and the mechanisms behind them.

Insulin aggregation studied using both $DiSC_2(3)$ and ThT

To explore the general applicability of this approach, we also studied the aggregation of insulin using phasor analysis of fluorescence decays recorded from the molecular rotor $DiSC_2(3)$. The data obtained for these experiments, shown in Fig. 6, exhibit a qualitatively similar behaviour to that observed for lysozyme. In particular, fluorescence lifetime images (Fig. 6a) revealed the formation and stabilisation of micron scale superstructures over the course of the aggregation reaction, along with an increase in the fluorescence lifetime indicating an increase in effective viscosity. Note that images (iii) and (iv) appear quite similar but have noticeably different phasor points (Fig. 6b), indicating that the viscosity increase continues even once the fibril network has almost completely formed. Moreover, three stages were observed on the phasor plot (Fig. 6b) in a manner closely analogous to the data for lysozyme. This observation highlights the generic nature of protein aggregation processes and suggests that our technique will be useful for studies of amyloid formation in a wide range of proteins.

Interestingly, the final phasor point in the insulin aggregation sits further from the universal circle than the final point observed for lysozyme (Fig. 3b), suggesting that two (or more) components remain present at the end of the insulin aggregation. The final insulin aggregation time point exhibited a bi-exponential decay and the long lifetime component of this decay – which reports on the fibrillar components of the aggregation mixture – was found to be 1.37 ns, corresponding to a viscosity of 275 cP. This is lower than the final viscosity observed during the lysozyme aggregation carried out at the same NaCl concentration (420 cP, Figs. 2a and 3a&b) and may indicate that insulin fibrils are packed less tightly than lysozyme fibrils. Alternatively, it is possible $DiSC_2(3)$ interacts less strongly with insulin fibrils than it does with lysozyme fibrils. However, we note that the maximum lifetime observed for $DiSC_2(3)$ in a very rigid environment (1:1 *v*/*v* methanol/ethanol, 77K glass) is 2.5 ns, significantly larger than the lifetimes recorded here for fully formed fibrillar mixtures. As such, these much lower values are unlikely to correspond to binding (which will cause immobilisation of $DiSC_2(3)$) and most likely reflect a reduction in solution free volume due to the formation of large fibrillar aggregates.

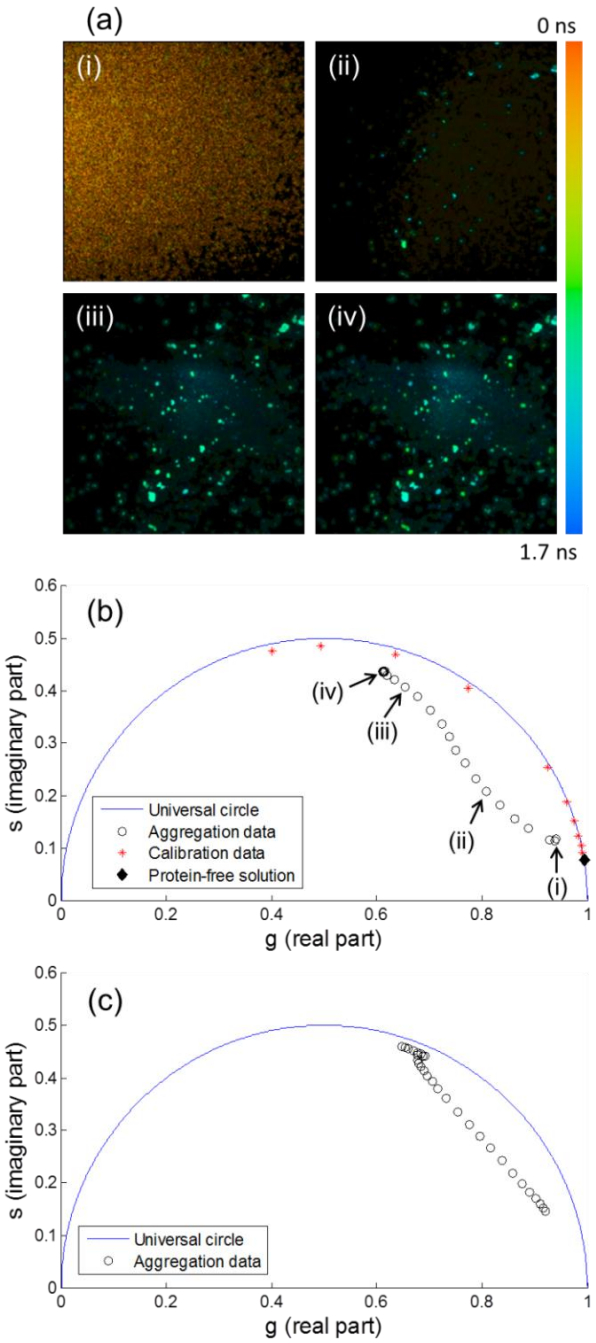

Figure 6. Multiphoton fluorescence lifetime imaging microscopy and phasor analysis of $DiSC_2(3)$ and ThT in aggregating insulin. Fluorescence lifetime images (**a**) and phasor plot (**b**) from a representative insulin aggregation (2 mg/ml monomeric insulin, 100 mM NaCl, 50 mM HCl, 0.2% v/v DMSO, unseeded) monitored by $DiSC_2(3)$ fluorescence. Images were recorded every 30 s (with a 30 s acquisition time) for 30 minutes. Phasor transforms were calculated for each image and the weighted centroids of each transform are shown in (**b**). Annotations on the phasor plot indicate the phasor centroids corresponding to the fluorescence lifetime images shown in (**a**). The filled black diamond represents the phasor for a fluorescence decay recorded in the reaction solution in the absence of protein (50 mM HCl, 100 mM NaCl only). **c**, Phasor plot obtained from an aggregation reaction carried out under identical conditions monitored using ThT.

In insulin, a similar phasor trajectory to that observed using $DiSC_2(3)$ is also obtained with ThT (Fig. 6c). This result is in agreement with the work of Mohanty *et al*[9] that detected three lifetime components in the fluorescence decay of ThT during the aggregation of insulin and suggests that the interaction between amyloid fibrils and ThT is weaker in insulin than it is in lysozyme. This allows ThT to function in a similar manner to $DiSC_2(3)$ (i.e. it allows ThT to sense multiple distinct stages of insulin aggregation). This result highlights the fact that ThT does not have equal affinity for all amyloid fibrils. Indeed, our results clearly show that, while the binding between ThT and lysozyme is very strong, this is not the case in insulin. It is also noteworthy that ThT decays are best fitted with a bi-exponential function even in completely homogeneous solutions[10] and, as such, the interpretation of a tri-exponential decay observed for ThT in insulin aggregation mixtures in reference [9] is not straightforward and does not necessarily indicate the presence of three aggregation components. Importantly, the phasor analysis approach used here allows us to unambiguously unravel this complexity and confirm that a minimum of three species contribute to the aggregation reaction.

Overall, our results suggest that combining a functioning molecular rotor (i.e. one whose viscosity sensitivity is not masked by strong, specific binding to the end product) with the use of phasor analysis has the potential to reveal novel and unique information about the processes and constituents involved in the aggregation of both lysozyme and insulin. Using ThT, this additional information is available when studying insulin solely through the use of phasor analysis (instead of standard fluorescence intensity based techniques). When monitoring the aggregation of lysozyme with ThT, however, phasor analysis yields no new information due to the strong binding that exists between ThT and fibrillar lysozyme. Importantly, our results show that $DiSC_2(3)$ is able to provide novel information (i.e. measurements of the viscosity and the number of aggregation components) in both insulin and lysozyme. This is because the interaction of $DiSC_2(3)$ with amyloid fibrils is weak or comparable in strength to its interaction with other aggregation components. As such, $DiSC_2(3)$ reveals important new insights into the formation of amyloid structures in both of the protein systems studied here.

CONCLUSIONS

One of the major challenges in understanding the phenomenon of amyloid aggregation is the complexity of the molecular pathways that underlie this process. Conventional light switch dyes such as ThT have been widely used and have yielded insights into the kinetics of fibril formation. However, by their very nature such methods provide one dimensional intensity data. In order to fundamentally increase the level of information obtainable through fluorescent reporters,

we have demonstrated the use of molecular rotors to obtain two dimensional data on protein aggregation in concentration/viscosity space. We have followed the dynamics of the aggregation of lysozyme and insulin by monitoring the fluorescence lifetime of $DiSC_2(3)$, a molecular rotor sensitive to the viscosity of its local environment. In the case of lysozyme, this marker was able to detect three sequential pathways leading to the formation of an aggregated protein gel, while only one aggregation stage was directly observable using ThT. Interestingly, both ThT and $DiSC_2(3)$ detected multiple stages in the aggregation of insulin. This indicates that other molecular rotors may also be useful in the study of amyloid formation. The applicability of a certain rotor, however, needs to be tested for each protein system, the requirement being that the rotor does not interact too strongly with the fully formed fibrils. Our results suggest that $DiSC_2(3)$ in particular may be useful in the study of a wide range of protein systems as it was observed to interact only weakly with both lysozyme and insulin. It also provided important new insights into the aggregation mechanism in both cases.

Using the molecular rotor based approach it was possible to follow both the change in fluorescence intensity and the local microviscosity. Additionally, through the use of phasor analysis, we were able to identify distinct stages in the aggregation process. Initially a simple transition between monomeric and fibrillar states was observed to take place; at later times, a change in the rate of viscosity increase was observed, and coincided with the appearance of micron size structures in fluorescence microscopy images. Overall, our results indicate the presence of complex aggregation pathways that are not revealed by monitoring the fluorescence intensity of ThT.

In conclusion, we have shown that the combination of phasor analysis and molecular rotors significantly enhances the level of information reported on the physical state of an aggregating protein system relative to the current state-of-the-art. We have demonstrated this using multiphoton fluorescence lifetime imaging microscopy, however, it could equally be achieved in a standard cuvette-based system. Furthermore, this approach can be extended in the future to live cell studies, which would involve covalently attaching a chosen molecular rotor to the protein of interest and this work is currently underway in our laboratory.

In summary, the method presented here has the capability to provide important insights into both the microrheological properties of amyloid materials and the mechanisms behind their formation. We believe that it will become useful in the study of neurodegeneration and in the development of functional proteinaceous nanomaterials based on amyloid structures.

METHODS

Viscosity calibration of $DiSC_2(3)$

Ten spectroscopic grade methanol-glycerol mixtures were prepared in the range 0-100% glycerol (weight/volume) and maintained at room temperature. The viscosity of each mixture was measured using a Stabinger viscometer (SVM 3000, Anton Paar, USA). $DiSC_2(3)$ (36809, Fluka Analytical, Switzerland) in DMSO was added to the methanol-glycerol mixtures at 13.9 µM and fluorescence decays were recorded using a multiphoton microscope (described below; 960 nm excitation, 525-700 nm emission). Decay traces (Fig. 1a) were fit to a mono-exponential model using TRI2 fitting software (Version 2.7, Gray Institute for Radiation Oncology and Biology, University of Oxford)[34] and fluorescence lifetimes were correlated to solution viscosity (Fig. 1b), permitting subsequent conversion between measured fluorescence lifetimes and viscosities. We observed a linear relationship between the logarithms of fluorescence lifetime and viscosity over the whole viscosity range investigated (0.6-930 cP), see Fig. 1b. Phasor transforms of each of the calibration decays were calculated (Fig. 3b). The phasors follow an anti-clockwise trajectory close to the universal circle as the viscosity increases.

Protein sample preparation

Lysozyme aggregation time courses were performed using hen egg white lysozyme. Monomeric lysozyme solutions were prepared under conditions of low pH: 4 mg/ml lysozyme, 50 mM HCl, 50-200 mM NaCl, and 0.2% v/v DMSO. The monomer solutions were passed through a 0.22 µm syringe-driven filter before use. The aggregation process was accelerated by the addition of preformed seed fibrils, constituting 2.4% w/w of the total lysozyme concentration in the reaction mixture (1% v/v). The seed fibrils were prepared by incubating a 10 mg/ml lysozyme solution (50 mM HCl, 100 mM NaCl) overnight at 65°C. The resulting aggregates were then sonicated on ice using a probe sonicator to obtain short seed fibrils, which were diluted 1:100 v/v into the sample. For the measurement of the pure seed sample, the sonicated seed fibrils were diluted 1:100 v/v into a 50 mM HCl, 100 mM NaCl solution. Insulin aggregation time courses were performed as above using 2 mg/ml monomeric bovine pancreas insulin (100 mM NaCl, 50 mM HCl, 0.2% DMSO, unseeded). The $DiSC_2(3)$ and ThT stock solutions were prepared in DMSO and water respectively. Hence, all reactions monitored using $DiSC_2(3)$ contained 0.2% v/v DMSO, which was shown to have no effect on the rate of aggregation (as monitored by ThT). Monomeric hen egg white lysozyme (L6786) and bovine pancreas insulin (I5500) were purchased from Sigma-Aldrich in powdered form. The pH of the reaction mixture was less than 2 for all experiments.

ThT aggregation assays

For aggregation assays monitored by ThT fluorescence, 20 μM ThT was added to the sample. Triplicates were incubated in a fluorimeter at 56°C and the fluorescence at 480 nm was monitored in response to 440 nm excitation.

Fluorescence lifetime measurements

Fluorescence lifetime measurements of protein aggregations were performed using either 3 μM $DiSC_2(3)$ or 20 μM ThT. 200 μl samples were mounted in a heated chamber (E200, Lauda GmbH, Germany) at 56°C and multiphoton fluorescence images/decays were recorded every 0.5-5 minutes during aggregation. Imaging was achieved using a confocal microscope (TCS SP5 II, Leica Microsystems GmbH, Germany) with an external Titanium:Sapphire laser (Chameleon Vision II, Coherent Ltd., UK), which provided pulsed excitation permitting 2-photon time-resolved fluorescence imaging (λ_{ex} = 960 nm for $DiSC_2(3)$; λ_{ex} = 880 nm for ThT). Fluorescence was recorded over the entire emission spectrum of $DiSC_2(3)$ (525-700 nm) and over the range 465-540 nm for ThT.

Fluorescence lifetime data analysis

Fluorescence decays were fit to mono- or bi-exponential decay models according to

$$I(t) = \sum_{i=1}^{n} \alpha_i \exp\left(-t/\tau_i\right), \qquad (1)$$

where I is fluorescence intensity, t is time, and α_i and τ_i are respectively the amplitudes and fluorescence lifetimes of the n exponentially decaying components. Fitting was achieved using either SPCImage (Becker & Hickl GmbH, Germany) or TRI2 analysis software. Lifetimes calculated using both programs were in agreement. Fluorescence lifetime images were produced using mono-exponential fitting and displayed using a false colour scale. To improve the signal-to-noise ratio (SNR) or to reduce acquisition times we chose to bin all image pixels into single decays or to record single decays rather than images during aggregations. In these cases, the higher SNR made bi-exponential fitting possible. The fractional contributions and lifetimes of the two fitted decay components were plotted as functions of time, as was the mean lifetime (τ_{mean}), calculated as

$$\tau_{mean} = \frac{\alpha_1\tau_1^2 + \alpha_2\tau_2^2}{\alpha_1\tau_1 + \alpha_2\tau_2}. \qquad (2)$$

To achieve accurate fitting it is necessary to deconvolve the measured data from the instrument response function (IRF). The IRF was estimated by recording the instantaneous second harmonic generation signal from a sample of urea crystals (960 nm excitation, 470-490 nm detection for $DiSC_2(3)$ experiments; 880 nm excitation, 430-450 nm detection for ThT experiments).

Phasor analysis was performed on the images/traces recorded for all aggregations using software written in-house in Matlab® (MathWorks™). Phasor analysis is a Fourier domain technique that involves plotting the real and imaginary components of the Fourier transform of a fluorescence decay[27] to provide an alternative 2-dimensional representation of the data. The real (g) and imaginary (s) components are calculated as:

$$g(\omega) = \frac{\int_0^\infty I(t)\cos(\omega t)dt}{\int_0^\infty I(t)dt} \qquad (3)$$

$$s(\omega) = \frac{\int_0^\infty I(t)\sin(\omega t)dt}{\int_0^\infty I(t)dt}. \qquad (4)$$

Here ω is the angular repetition frequency of the pulsed excitation laser (2π x 80 MHz), t is time and $I(t)$ is the measured fluorescence decay profile. Phasors of mono-exponential decays lie on the 'universal circle' (a semicircle centred at g = ½, s = 0), while multi-exponential decays produce phasors inside the universal circle. For each fluorescence lifetime image, the phasor transform appears as a diffuse cloud (Supplementary Fig. 3a) indicating the spread of fluorescence lifetimes. To summarise the phasor plot for each image, we calculated the weighted centroid of the phasor cloud using the Matlab® 'regionprops' function. Plotting the weighted centroids of the phasor plots at all aggregation time points allowed us to determine the minimum number of discrete components contributing to the decays. For example, in the case of conversion between two fixed mono-exponential components, the phasors of the reaction mixture will follow a straight line joining the phasors of the two fixed components. In this way, we determined the minimum number of species (of different viscosities) involved in the aggregation process.

ASSOCIATED CONTENT

Supporting information. Supplementary figures and description of numerical simulations. This material is available free of charge via the Internet at http://pubs.acs.org.

AUTHOR INFORMATION

Corresponding authors

* m.kuimova@imperial.ac.uk
* tpjk2@cam.ac.uk

Author contributions

All authors have given approval to the final version of the manuscript.

† These authors contributed equally to this work.

Notes

The authors declare no competing financial interests.

ACKNOWLEDGEMENTS

We thank the Engineering and Physical Sciences Research Council (EPSRC, UK) for financial support. Marina K. Kuimova acknowledges the EPSRC for a Career Acceleration Fellowship (grant number: EP/I003983/1).

REFERENCES

1. Dobson, C. M. Protein Misfolding, Evolution and Disease, *Trends Biochem. Sci.* **1999**, 24, 329-332.
2. Chiti, F.; Dobson, C. M. Protein Misfolding, Functional Amyloid, and Human Disease. *Annu. Rev. Biochem.* **2006**, 75, 333-366.
3. Hartl, F. U; Hayer-Hartl, M. Converging Concepts of Protein Folding in Vitro and in Vivo. *Nat. Struct. Mol. Biol.* **2009**, 16, 574-581.
4. Knowles, T. P. J.; Buehler, M. J. Nanomechanics of Functional and Pathological Amyloid Materials. *Nat. Nanotechnol.*,**2011**, 6, 469-479.
5. Cook, N. P.; Kilpatrick, K.; Segatori, L.; Marti, A. A. Detection of alpha-Synuclein Amyloidogenic Aggregates in Vitro and in Cells Using Light-Switching Dipyridophenazine Ruthenium(II) Complexes. *J. Am. Chem. Soc.* **2012**, 134, 20776-20782.
6. Voropai, E. S.; Samtsov, M. P.; Kaplevskii, K. N.; Maskevich, A. A.; Stepuro, V. I.; Povarova, O. I.; Kuznetsova, I. M.; Turoverov, K. K.; Fink, A. L.; Uverskii, V. N. Spectral Properties of Thioflavin T and Its Complexes with Amyloid Fibrils. *J. Appl. Spectrosc.* **2003**, 70, 868-874.
7. Maskevich, A. A.; Stsiapura, V. I.; Kuzmitsky, V. A.; Kuznetsova, I. M.; Povarova, O. I.; Uversky, V. N.; Turoverov, K. K. Spectral Properties of Thioflavin T in Solvents with Different Dielectric Properties and in a Fibril-Incorporated Form. *J. Proteome Res.* **2007**, 6, 1392-1401.
8. Cohen, S. I.; Linse, S.; Luheshi, L. M.; Hellstrand, E.; White, D. A.; Rajah, L.; Otzen, D. E.; Vendruscolo, M.; Dobson, C. M.; Knowles, T. P. Proliferation of Amyloid-beta42 Aggregates Occurs Through a Secondary Nucleation Mechanism. *Proc. Natl. Acad. Sci. U. S. A.* **2013**, 110, 9758-9763.
9. Mohanty, J.; Choudhury, S. D.; Pal, H.; Bhasikuttan, A. C. Early Detection of Insulin Fibrillation: a Fluorescence Lifetime Assay to Probe the Pre-fibrillar Regime, *Chem. Commun. (Camb)* **2012**, 48, 2403-2405.
10. Stsiapura, V. I.; Maskevich, A. A.; Kuzmitsky, V. A.; Uversky, V. N.; Kuznetsova, I. M.; Turoverov, K. K. Thioflavin T as a Molecular Rotor: Fluorescent Properties of Thioflavin T in Solvents with Different Viscosity. *J. Phys. Chem. B*, **2008**, 112, 15893-15902.
11. Sigurdson, C. J.; Nilsson, K. P.; Hornemann, S.; Manco, G.; Polymenidou, M.; Schwarz, P.; Leclerc, M.; Hammarstrom, P.; Wuthrich, K.; Aguzzi, A. Prion Strain Discrimination Using Luminescent Conjugated Polymers, *Nat. Methods*, 2007, **4**, 12, 1023-1030.
12. Lee, J.; Culyba, E. K.; Powers, E. T.; Kelly, J. W. Amyloid-beta Forms Fibrils by Nucleated Conformational Conversion of Oligomers. *Nat. Chem. Biol.* **2011**, 7, 602-609.
13. Amaro, M.; Birch, D. J.; Rolinski, O. J. Beta-Amyloid Oligomerisation Monitored by Intrinsic Tyrosine Fluorescence. *Phys. Chem. Chem. Phys.* **2011**, 13, 6434-6441.
14. Chan, F. T.; Kaminski Schierle, G. S.; Kumita, J. R.; Bertoncini, C. W.; Dobson, C. M.; Kaminski, C. F. Protein Amyloids Develop an Intrinsic Fluorescence Signature During Aggregation. *Analyst* **2013**, 138, 2156-2162.
15. Tjernberg, L. O.; Pramanik, A.; Bjorling, S.; Thyberg, P.; Thyberg, J.; Nordstedt, C.; Berndt, K. D.; Terenius, L.; Rigler, R. Amyloid beta-Peptide Polymerization Studied Using Fluorescence Correlation Spectroscopy. *Chem. Biol.* **1999**, 6, 53-62.
16. Brown, C. M.; Dalal, R. B.; Hebert, B.; Digman, M. A.; Horwitz, A. R.; Gratton, E. Raster Image Correlation Spectroscopy (RICS) for Measuring Fast Protein Dynamics and Concentrations with a Commercial Laser Scanning Confocal Microscope. *J. Microsc.* **2008**, 229, 78-91.
17. Hamrang, Z.; Pluen, A.; Zindy, E.; Clarke, D. Raster Image Correlation Spectroscopy as a Novel Tool for the Quantitative Assessment of Protein Diffusional Behaviour in Solution. *J. Pharm. Sci. U. S.* **2012**, 101, 2082-2093.
18. Sabate, R.; Saupe, S. J. Thioflavin T Fluorescence Anisotropy: An Alternative Technique for the Study of Amyloid Aggregation. *Biochem. Biophys. Res. Commun.* **2007**, 360, 135-138.
19. Jha, A.; Udgaonkar, J. B.; Krishnamoorthy, G. Characterization of the Heterogeneity and Specificity of Interpolypeptide Interactions in Amyloid Protofibrils by Measurement of Site-Specific Fluorescence Anisotropy Decay Kinetics. *J. Mol. Biol.* **2009**, 393, 735-752.
20. Roberti, M. J.; Jovin, T. M.; Jares-Erijman, E. Confocal Fluorescence Anisotropy and FRAP Imaging of alpha-Synuclein Amyloid Aggregates in Living Cells. *PLoS One* **2011**, 6, e23338
21. Shammas, S. L.; Garcia, G. A.; Kumar, S.; Kjaergaard, M.; Horrocks, M. H.; Shivji, N.; Mandelkow, E.; Knowles, T. P.; Mandelkow, E.; Klenerman, D. A Mechanistic Model of Tau Amyloid Aggregation Based on Direct Observation of Oligomers. *Nat. Commun.* **2015**, 6, 7025.
22. Kuimova, M. K. Mapping Viscosity in Cells Using Molecular Rotors. *Phys. Chem. Chem. Phys.* **2012**, 14, 12671-12686.
23. Haidekker, M. A.; Theodorakis, E. A. Environment-Sensitive Behavior of Fluorescent Molecular Rotors. *J. Biol. Eng.* **2010**, 4: 11
24. Förster, T. ; Hoffmann, G. Viscosity Dependence of Fluorescent Quantum Yields of Some Dye Systems. *Z. Phys. Chem.* **1971**, 75, 63-76.
25. Amdursky, N.; Erez, Y.; Huppert, D. Molecular Rotors: What Lies Behind the High Sensitivity of the Thioflavin-T Fluorescent Marker. *Acc. Chem. Res.* **2012**, 45, 1548-1557.
26. Turoverov, K. K.; Kuznetsova, I. M.; Maskevich, A. A.; Stepuro, V. I.; Kuzmitsky, V. A.; Uversky, V. N. ThT as an Instrument for Testing and Investigation of Amyloid and Amyloid-like Fibrils, in: *International Conference on Lasers, Applications, and Technologies 2007: Environmental Monitoring and Ecological Applications; Optical Sensors in Biological, Chemical, and Engineering Technologies; and Femtosecond Laser Pulse Filamentation*, 2007, Bellingham, SPIE - Intl. Soc. Opt. Eng.: Bellingham, **2007**, 6733..
27. Digman, M. A.; Caiolfa, V. R.; Zamai, M.; Gratton, E. The Phasor Approach to Fluorescence Lifetime Imaging Analysis. *Biophys. J.* **2008**, 94, L14-16.
28. Pepys, M. B.; Hawkins, P. N.; Booth, D. R.; Vigushin, D. M.; Tennent, G. A.; Soutar, A. K.; Totty, N.;

Nguyen, O.; Blake, C. C. F.; Terry, C. J.; Feest, T. G.; Zalin, A. M.; Hsuan, J. J. Human Lysozyme Gene Mutations Cause Hereditary Systemic Amyloidosis. *Nature* **1993**, 362, 553-557.

29. Booth, D. R.; Sunde, M.; Bellotti, V.; Robinson, C. V.; Hutchinson, W. L.; Fraser, P. E.; Hawkins, P. N.; Dobson, C. M.; Radford, S. E.; Blake, C. C. F.; Pepys, M. B. Instability, Unfolding and Aggregation of Human Lysozyme Variants Underlying Amyloid Fibrillogenesis. *Nature*, **1997**, 385, 787-793.

30. Hosny, N. A.; Fitzgerald, C.; Tong, C.; Kalberer, M.; Kuimova, M. K.; Pope, F. D. Fluorescence Lifetime Imaging of Atmospheric Aerosols: A Direct Probe of Aerosol Viscosity. *Faraday Discuss.*, **2013**, 165, 343-356.

31. Arnaudov, L. N.; de Vries, R. Thermally Induced Fibrillar Aggregation of Hen Egg White Lysozyme. *Biophys. J.* **2005**, 88, 515-526.

32. Krebs, M. R. H.; Wilkins, D. K.; Chung, E. W.; Pitkeathly, M. C.; Chamberlain, A. K.; Zurdo, J.; Robinson, C. V.; Dobson, C. M. Formation and Seeding of Amyloid Fibrils from Wild-Type Hen Lysozyme and a Peptide Fragment from the beta-Domain. *J. Mol. Biol.* **2000**, 300, 541-549.

33. James, N. G.; Ross, J. A.; Stefl, M.; Jameson, D. M. Applications of Phasor Plots to in Vitro Protein Studies. *Anal. Biochem.* **2011**, 410, 70-76.

34. Barber, P. R.; Ameer-Beg, S. M.; Gilbey, J.; Carlin, L. M.; Keppler, M.; Ng, T. C.; Vojnovic, B. Multiphoton Time-Domain Fluorescence Lifetime Imaging Microscopy: Practical Application to Protein-Protein Interactions Using Global Analysis. *J. Royal Soc. Interface* **2009**, 6, S93-S105.